LA-UR-21-21491
Approved for public release; distribution is unlimited.

Title: A Diamagnetic-Loop-Based Beam Radius Monitor (BRM)

Author(s): Smith, Horace Vernon
Broste, William B.
Ekdahl, Carl August Jr.

Intended for: DARHT Technical Note No. 507

Issued: 2021-07-20 (rev.1)

DARHT Technical Note No. 507

July 13, 2021

A Diamagnetic-Loop-Based Beam Radius Monitor (BRM)

By

H. Vernon Smith, William B. Broste, and Carl A. Ekdahl,

LA-UR-21-21491

Los Alamos National Laboratory

Group J-6

This page intentionally left blank.

A Diamagnetic-Loop-Based Beam Radius Monitor (BRM)

H. Vernon Smith, William B. Broste, and Carl A. Ekdahl

Abstract

We describe a non-interceptive beam radius monitor that employs a diamagnetic loop. In order to increase the signal strength, the diamagnetic loop radius is considerably smaller than the outer wall radius, the device is placed inside a specially built solenoid magnet to allow independent adjustment of the guide magnetic field strength, and there are two counter-wound diamagnetic loops to double the signal strength and to eliminate common mode signals. This device is calibrated and the magnitude of the electron beam offset/tilt contribution to the measured radius estimated. This device is ready to be validated on an electron induction LINAC such a DARHT-I or DARHT-II.

Introduction

Refs. 1-4 describe the first proposals to use a diamagnetic loop (DML) to measure the rms radius of an intense, pulsed electron beam in an induction linac. Ref. 5 describes a successful measurement of the rms radius of the FXR beam at LLNL. Attempts at Los Alamos to use a diamagnetic loop to measure the DARHT-I and DARHT-II accelerator beam sizes gave mixed results.[6] A diamagnetic loop device was fabricated and calibrated at the Chinese Academy of Engineering Physics:[7] it was used it to measure the beam radius for a 2-MeV injector[8] and for the Dragon-I linear induction accelerator.[9, 10]

Although successfully demonstrated on DARHT-I, implementation of DMLs on DARHT-II suffered from excessive background noise due to their small detection area and their location in the weak fringe fields of the focusing solenoids. An improved DML apparatus is designed to avoid these compromises by providing a large sensitive area in a stand-alone magnetic field of appropriate strength.[11]

This technical note describes the improved diamagnetic loop device designed and constructed based on ref. 11. See Table 1 for a list of contributors to the work described in this report.

Diamagnetic-Loop-Based Beam Radius Monitor Design

Consider a beam with radial extent *a* centered in a perfectly conducting tube with radius R_{wall}. Before the beam enters the tube the initial value of the solenoidal guide field is B_0. After the beam enters the tube the guide field is depressed within the beam by its diamagnetism. The field outside of the beam is increased to $B_0 + \Delta B$, because flux is conserved inside of the tube. This geometry is illustrated in Fig. 1.

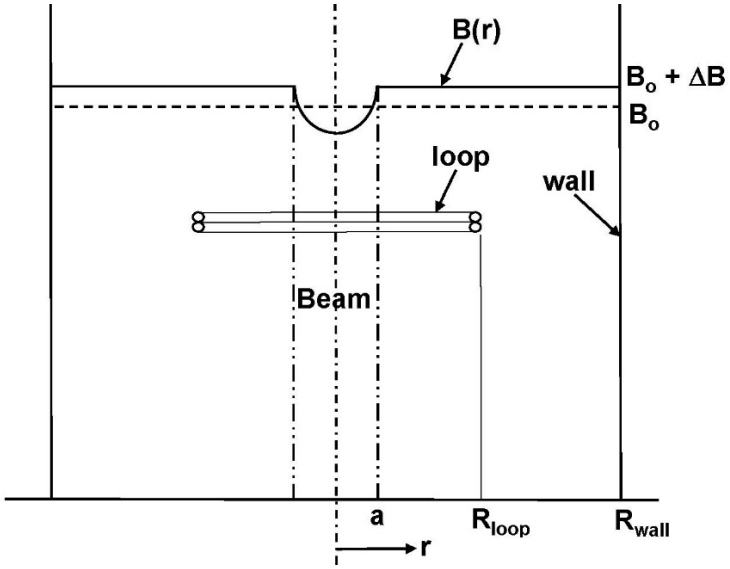

Figure 1. When a beam of radius a is transported through a beam pipe of radius R_{wall} the initial constant magnetic field B_o is modified as shown due to the beam's diamagnetism. A 2-turn loop with radius R_{loop} is used to measure the excluded flux.

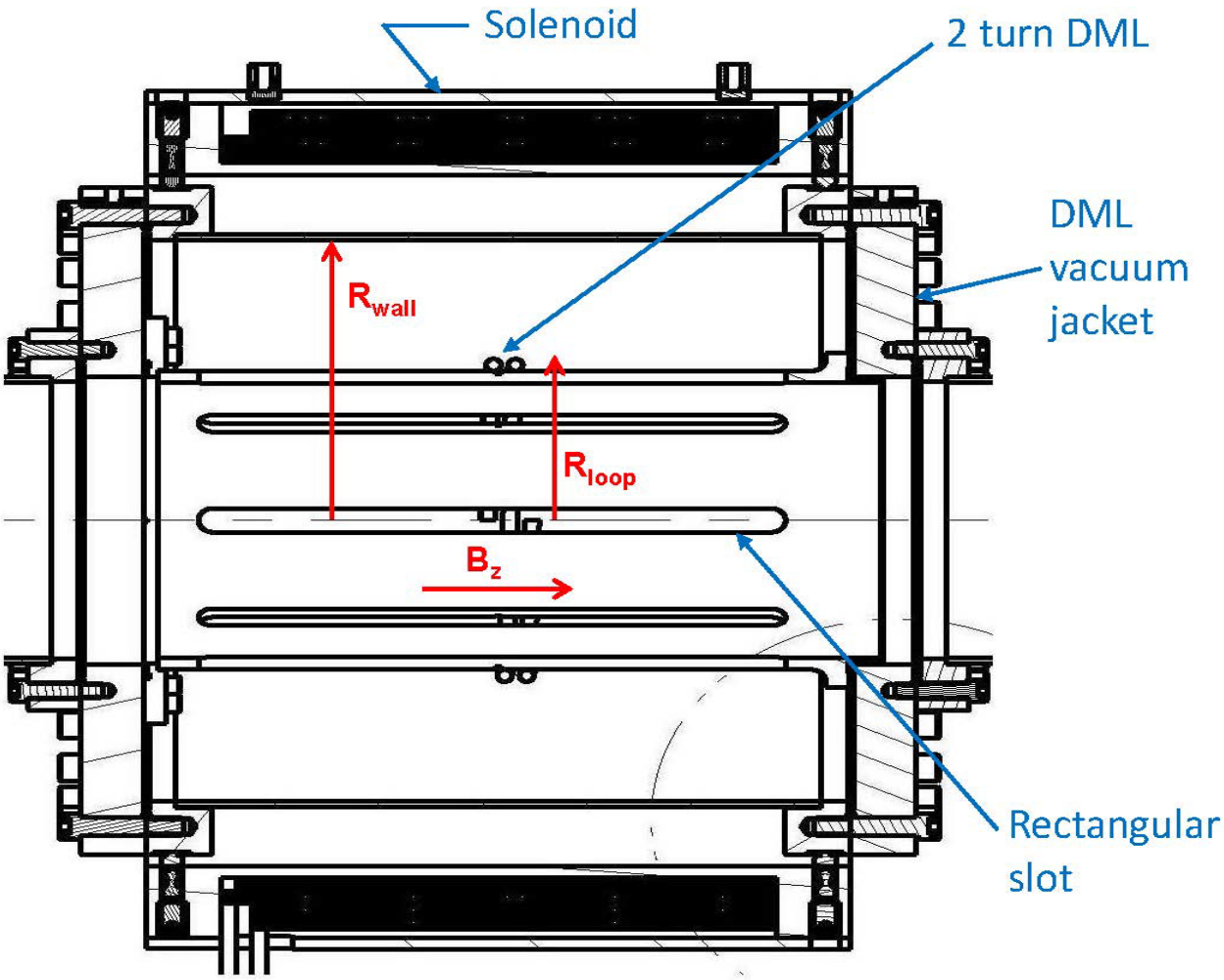

Figure 2. The geometry of the diamagnetic loop device.

It can be shown[12] that

$$V_{loop} = \pi R_{rms(beam)}^2 B_z \frac{dI_b / dt}{17\beta\gamma \mathrm{kA}} \left[1 - \frac{R_{loop}^2}{R_{wall}^2} \right] \quad (1)$$

where V_{loop} is the voltage induced across the diamagnetic loop, $R_{rms(beam)}$ is the rms radius of the beam passing through the diamagnetic loop, dI_b/dt is the instantaneous change in the beam current passing through the diamagnetic loop, B_z is the value of the guide field provided by the solenoid magnet external to the diamagnetic loop, R_{loop} is the radius of the diamagnetic loop coil, and R_{wall} is the inner radius of the beam pipe surrounding the diamagnetic loop apparatus (Fig. 2). The factor in brackets is just equal to the theoretical value of magnetic flux through the loop divided by the flux excluded by the beam in an axially uniform magnetic field inside a beam pipe of constant radius. It is the calibration factor that must be determined experimentally for any geometry that has axial variation.

Using $R_{rms(beam)}$ = 2 cm, B_z = 100 G, d I_b / dt = 1700 A/10 ns = 1.7 x 10^{11} A/s, E_{beam} = 20 MeV (β = 1 and γ = 39.7), and [1 – R_{loop}^2/R_{wall}^2] = 0.72 gives V_{loop} = 2.3 V for 1 diamagnetic loop and 4.6 V for 2 diamagnetic loops. See Table 2 for various DML dimensions.

The present diamagnetic loop design (see Table 3 for a list of approved drawings) uses three improvements over previous designs, all suggested by equation (1). First, the diamagnetic loop is placed in a solenoid magnet whose field strength can be adjusted to give a desired signal level as the detected signal strength is directly proportional to the external magnetic field. Previous designs have relied on stray magnetic fields from nearby beamline components. Second, the diamagnetic loop itself has a radius 0.53 times that of the housing inner wall, so the factor [1 – R_{loop}^2/R_{wall}^2] is 0.72, larger than that of previous designs where the loop radius is a larger fraction of the wall radius. Third, we employ two counter-wound diamagnetic loops to double the signal and to eliminate any common mode signals. The diameter of the DML wire is 1.02 mm (1.11 mm including insulation), R_{loop} = 7.918 cm, and R_{wall} = 14.92 cm.

A CAD drawing of the diamagnetic loop apparatus is shown in Fig. 3. An exploded view of the diamagnetic loop apparatus is shown in Fig. 4. A sketch of the diamagnetic loop apparatus is shown in Fig. 5. Non-magnetic materials (stainless steel and copper) are used throughout the fabricated apparatus.

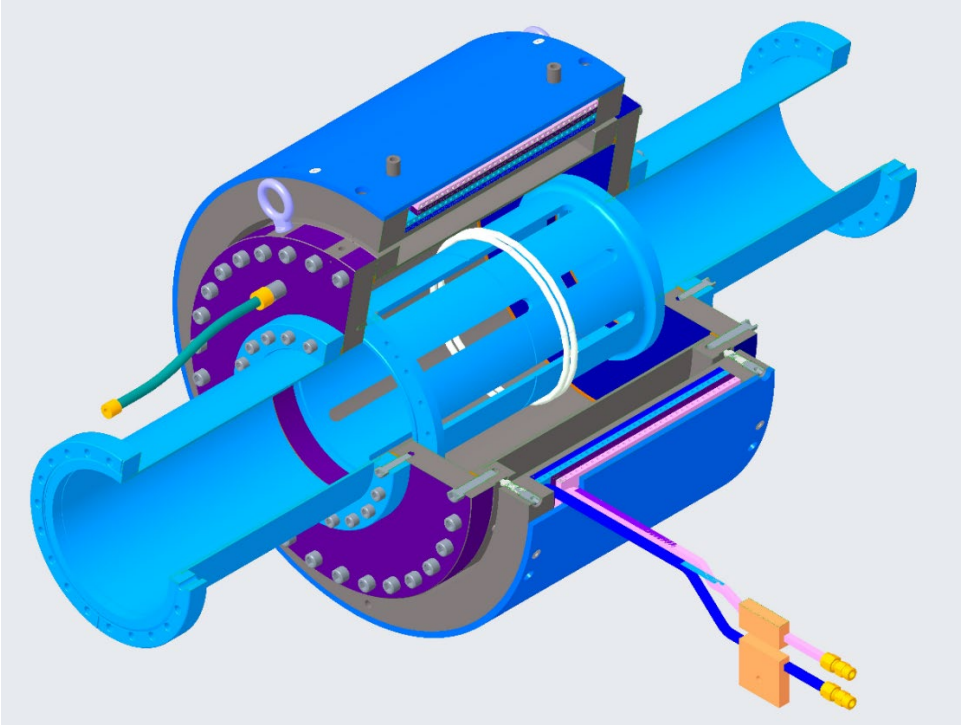

Figure 3. CAD drawing of the diamagnetic loop apparatus.

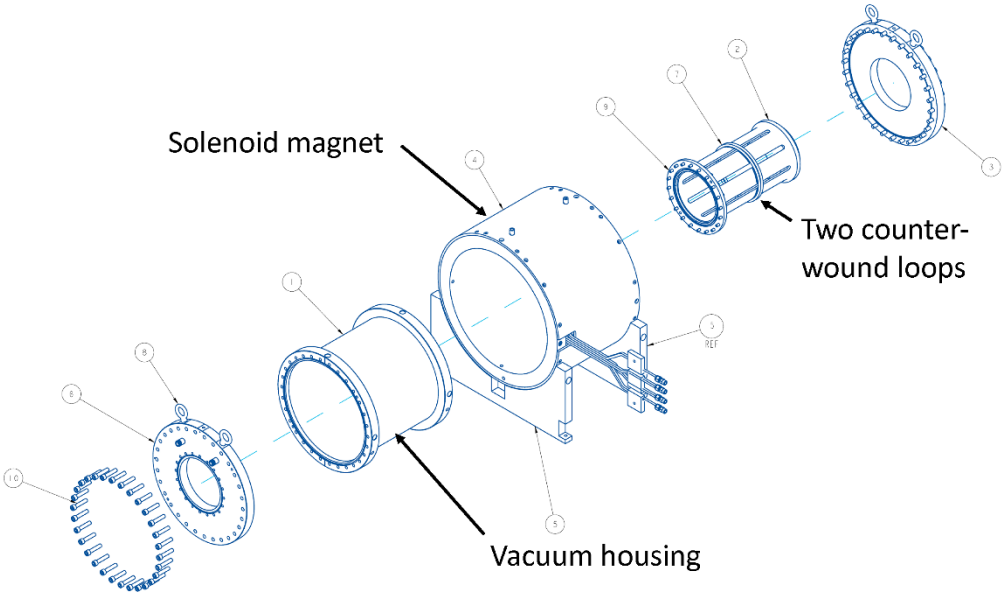

Figure 4. Exploded view of the Diamagnetic Loop apparatus.

There are eight 1.27-cm-wide x 25.4-cm-long slots machined in the mandrel which the two counter-wound loops are wrapped around (Figs. 2-4) to allow the loops to respond to the fast rise diamagnetic perturbation caused by the electron beam.

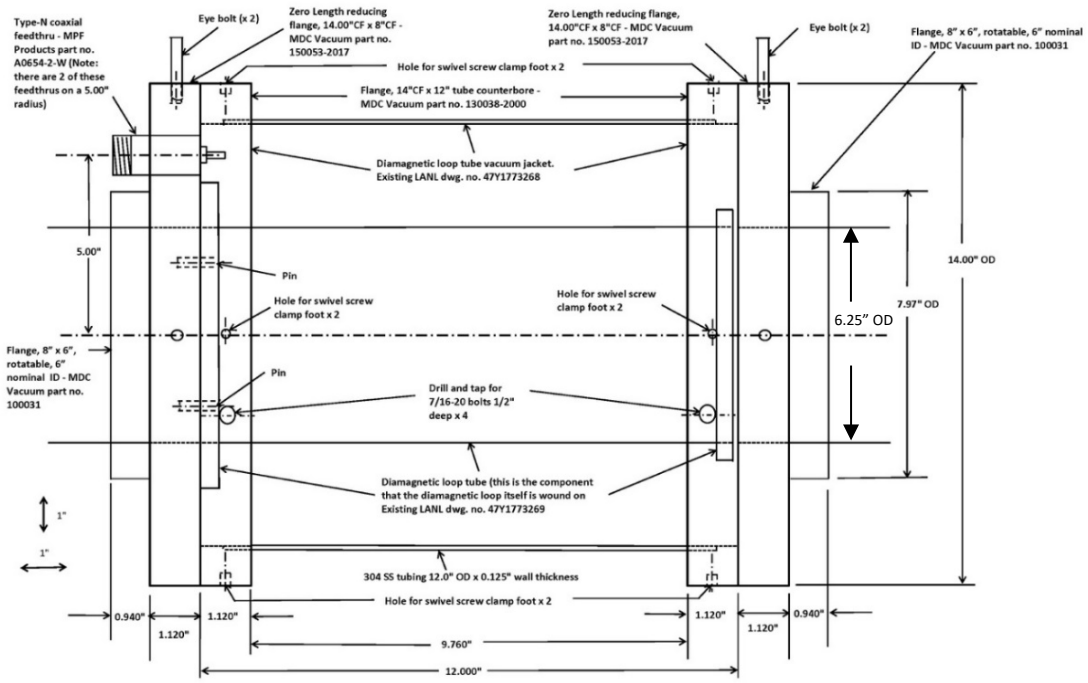

Figure 5. A sketch (side view) of the diamagnetic loop apparatus.

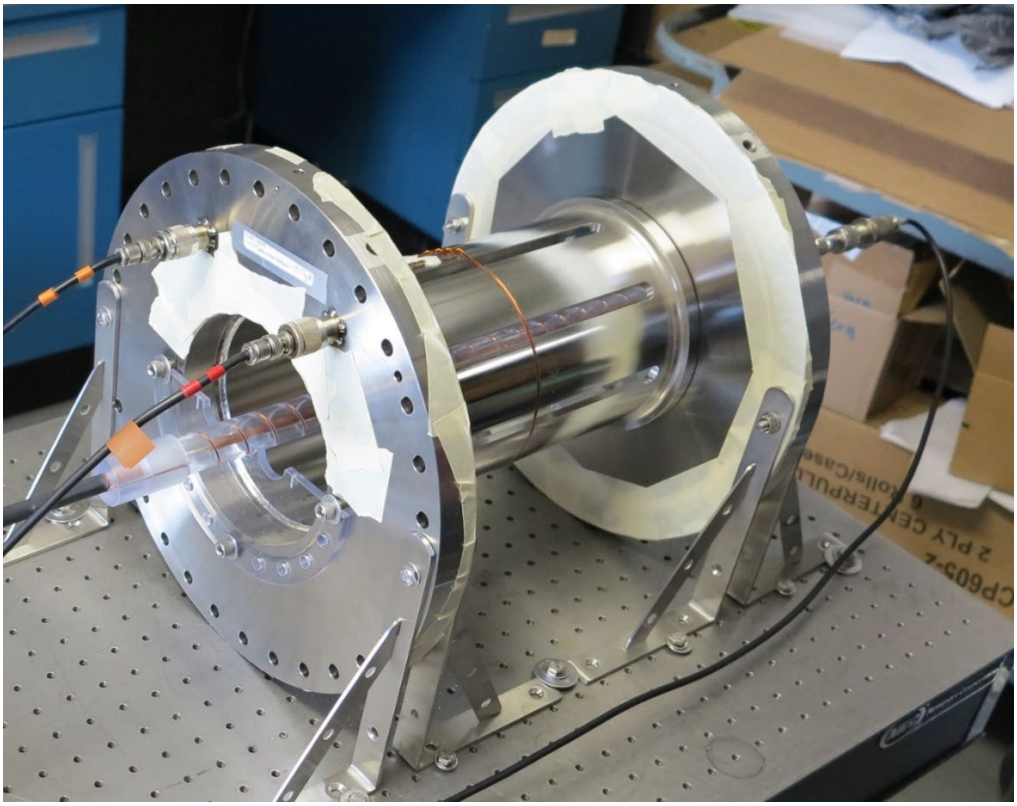

Figure 6. A photograph of the diamagnetic loop apparatus with the outer vacuum jacket removed. Clearly shown are the longitudinal slots in the mandrel that allow the rapidly varying axial field to fill the region between the DML and the flux conserving outer wall.

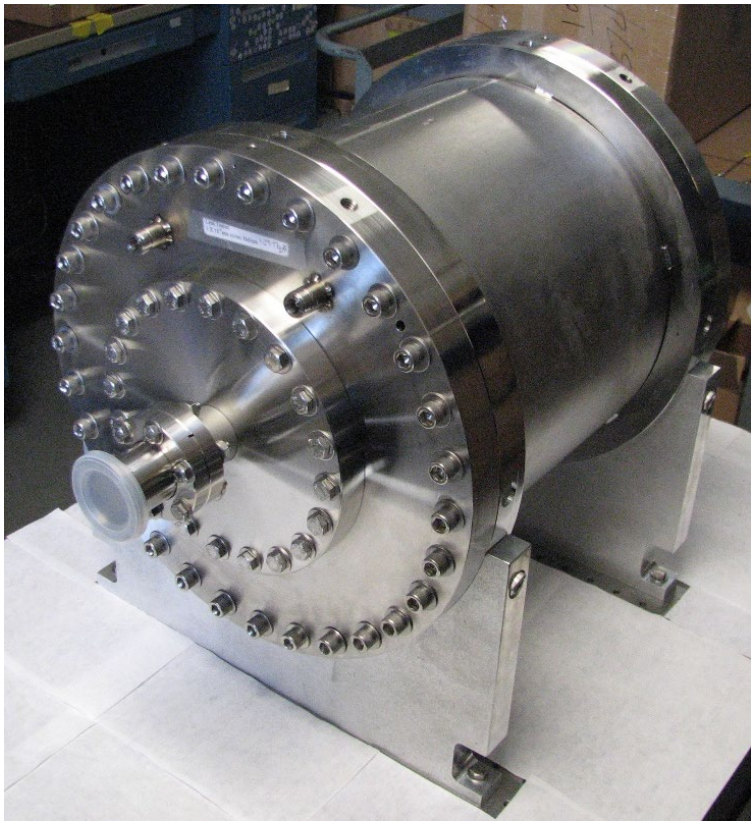

Figure 7. A photograph of the DML apparatus taken just before it was vacuum leak checked.

The diamagnetic loop assembly ready for vacuum leak checking is shown in Fig. 7. A Pfeiffer HLT 260 Qualytest leak detector was used to verify this assembly is leak tight.[13]

Guide Field Solenoid Magnet Design

The diamagnetic loop (Figs. 2-7) is immersed in a solenoidal magnetic field of known strength to allow calculation of the rms beam radius using the measured voltage induced across the diamagnetic loop. See Table 4 for a list of approved solenoid magnet drawings. This solenoid magnet (Figs. 8, 9) is also an optical device in the beam transport line. Fortunately, the strength of the magnetic field only needs to be ~100 Gauss in order to obtain a measurable voltage signal from the diamagnetic loop, so the magnet design can be simplified without having to take special precautions, such as quadrufilar windings[14] and homogenizer rings[15] as in the DARHT-I accelerator cell solenoid magnet design.[14] The dimensions for the 132 magnet windings are given in Table 2.

The formula for the field on axis of a solenoid is

$$B_o = \mu_o I n (\cos\beta - \cos\alpha) / 2 \qquad (2)$$

where B_o is the field generated on the axis of the solenoid with current I and n turns/cm (n = 5.530 turns/cm), μ_o is the permittivity of free space, $\cos\beta=(x+L/2)/[(x+L/2)^2+R^2]^{0.5}$, and $\cos\alpha=(x-L/2)/[(x-L/2)^2+R^2]^{0.5}$. x = 0 at the center of the magnet. We use the

mechanical dimensions of the magnet for L (= 24 cm) and R (= 20.6 cm) to calculate the magnetic field vs current. The result is shown as the green squares in Fig. 10. Note that eq. 2 is the equation for the magnetic field on axis of a solenoid formed by an infinitesimally thin current sheet: it is only an approximation for finite thickness windings.

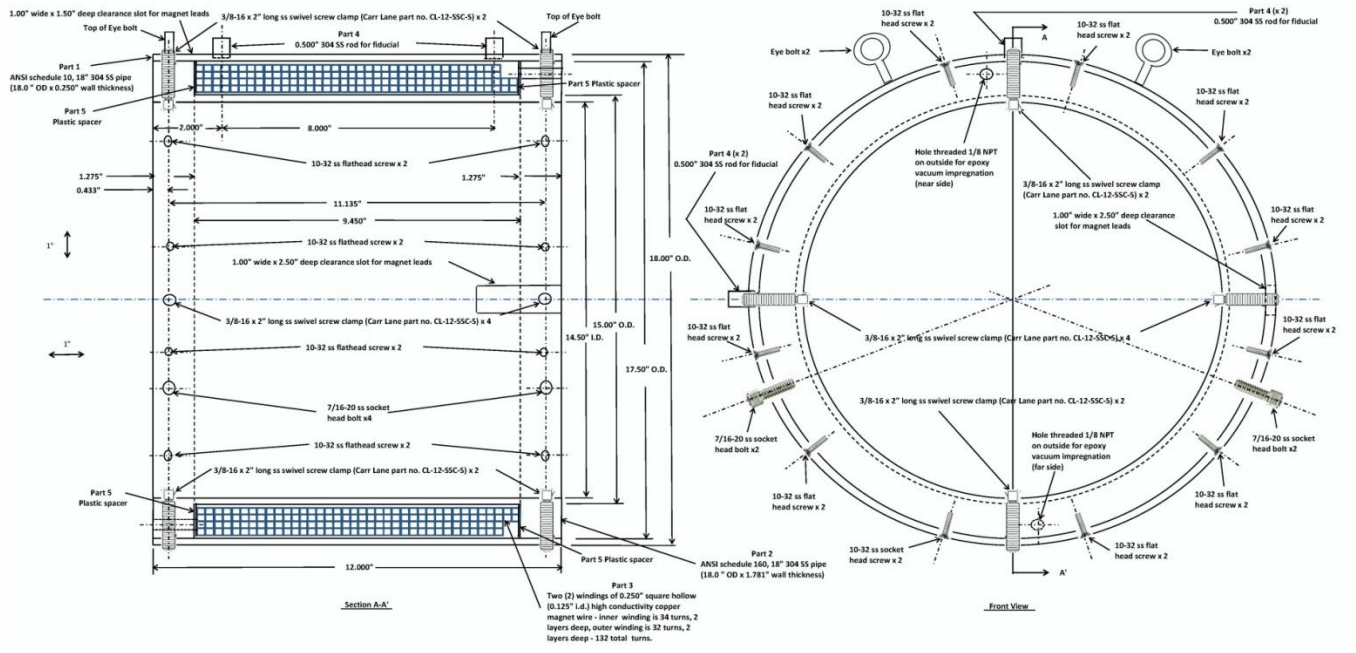

Figure 8. A sketch of the diamagnetic loop solenoid magnet.

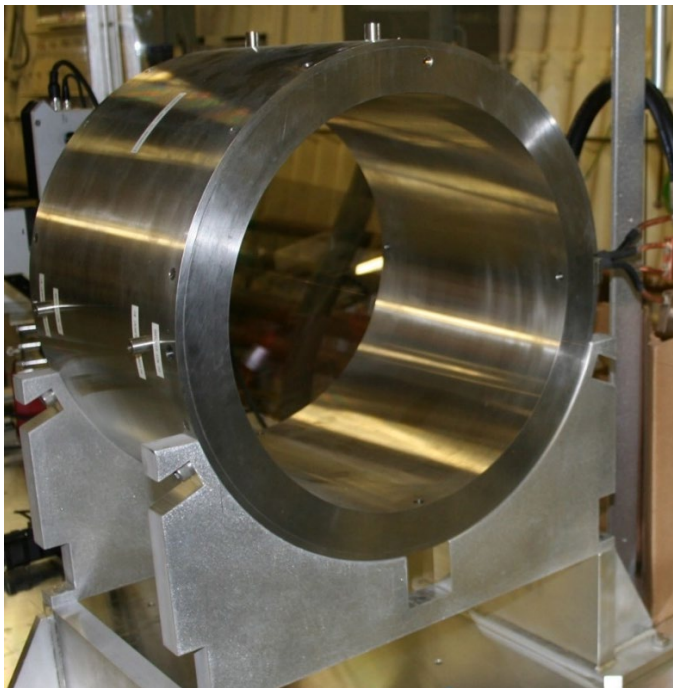

Figure 9. A photograph of the diamagnetic loop solenoid magnet.

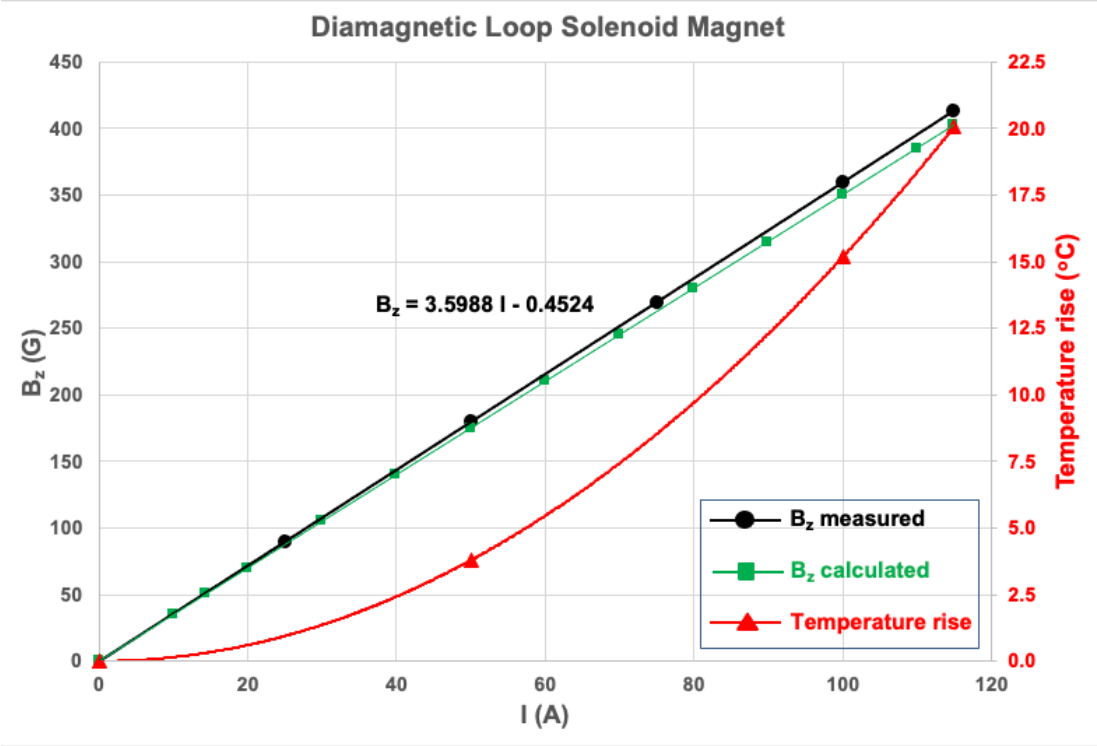

Figure 10. The calculated solenoid magnetic field on axis (green squares), the measured magnetic field on axis (black circles), and the magnet temperature rise (red triangles) as a function of the magnet coil current.

The solenoid magnet was mapped by the AOT-RFE magnet team.[16] The measured B_z vs I is shown as the black circles in Fig. 10. It only takes 28 A to generate a 100 G magnetic field. The solenoid magnet temperature rise as a function of I was calculated:[17] the results of this calculations are shown as the red triangles in Fig. 10.

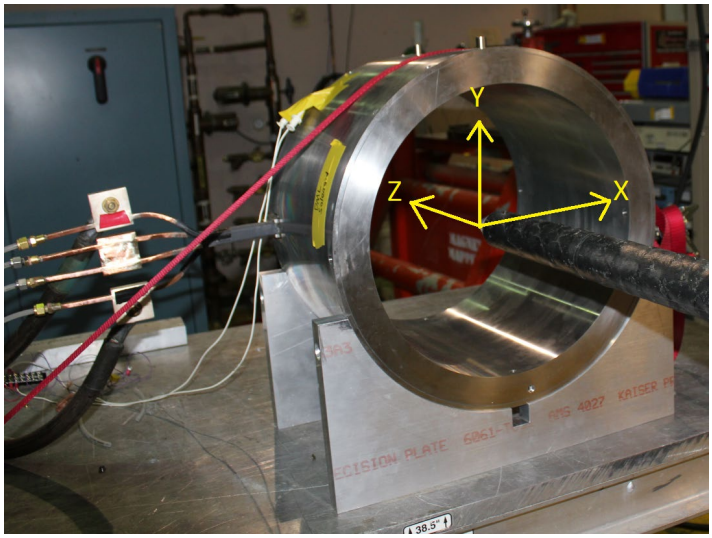

Figure 11. The coordinate system used for the point map measurements is left-handed. X=0, Y=0, and Z = 0 are at the mechanical center of the magnet.

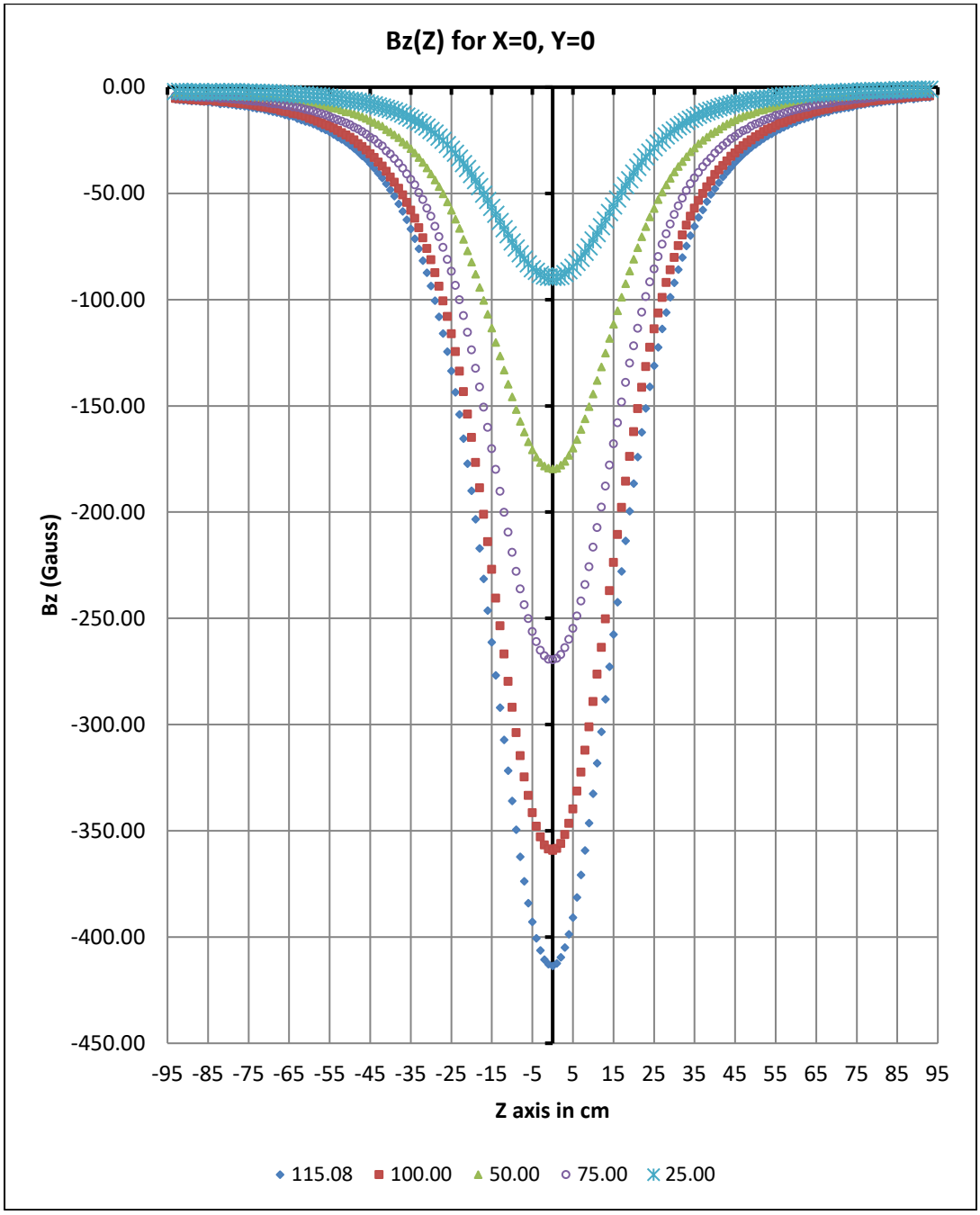

Figure 12. The measured axial solenoid magnetic field as a function of z for x=y=0.

The coordinate system uses for the point map measurements is shown in Fig. 11. The measured B_z vs z for x=y=0 is shown in Fig. 12. For magnet current = 50 A the measured B_z vs x for y=z=0 and for B_z vs y for x=z=0 is shown in Fig. 13. The mechanical center of the solenoid magnet is at x = 0, y = 0, and z = 0.

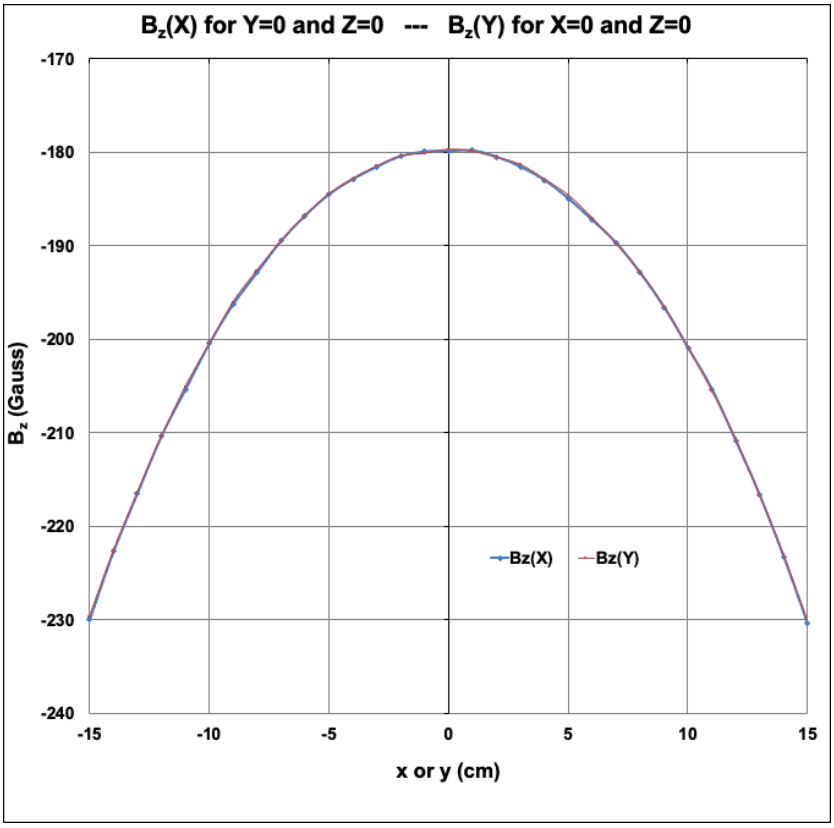

Figure 13. The measured axial magnetic field as a function of x for y=z=0 (blue) and as a function of y for x=z=0 (red). The magnet current is 50 A for these measurements.

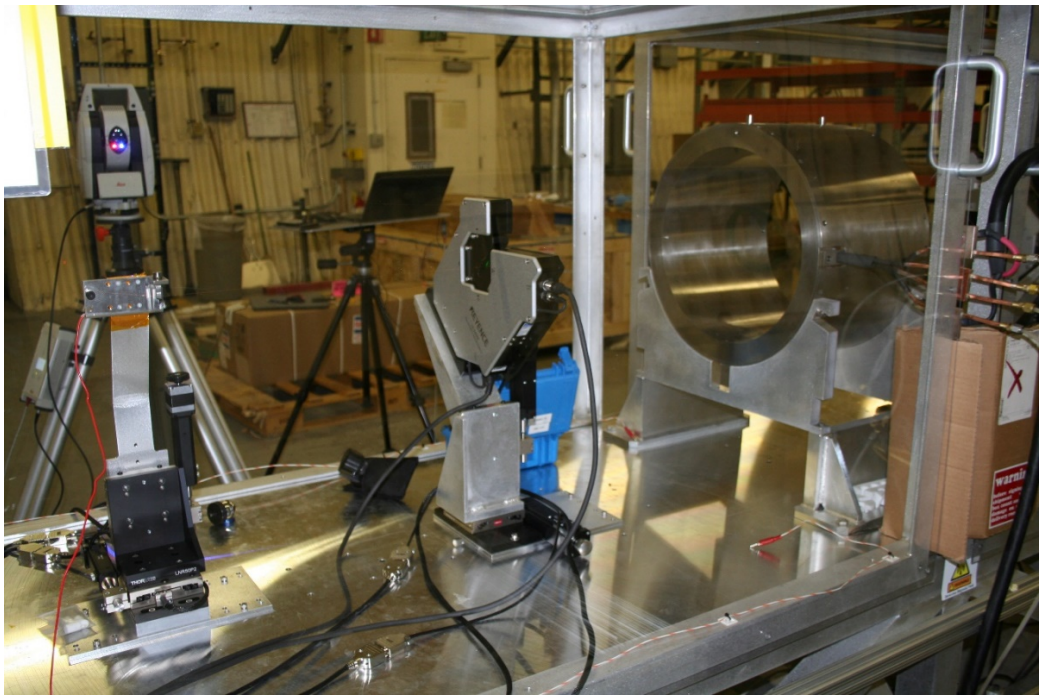

Figure 14. The DML solenoid magnet on the LANL vibrating wire SWAT stand.

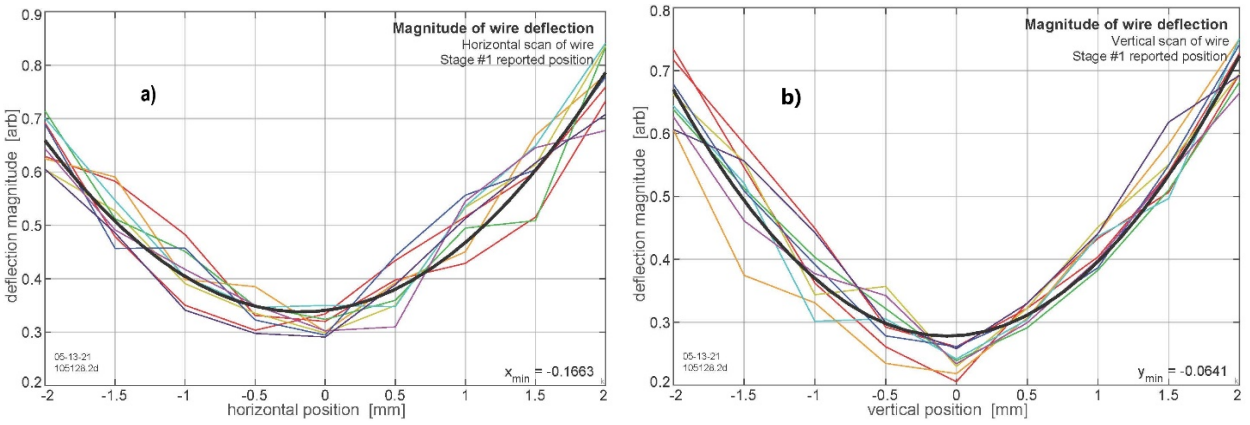

Figure 15. Measurement of a) the x magnetic axis position and b) the y magnetic axis position with respect to the solenoid mechanical axis.

The position (x, y) and tilt (yaw, pitch) of the solenoid magnetic field with respect to the solenoid mechanical axis is measured by the AOT-AE SWAT and AOT-MDE laser-tracker teams. A photograph of the solenoid magnet mounted on the pulsed, vibrating wire SWAT stand in MPF-365 at TA-53 is shown in Fig. 14. The measured deflection vs x for y=0 is shown in Fig. 15a: the measured deflection vs y for x = 0, in Fig. 15b. The x and y mechanical centers are both at 0 mm. For the measurement shown in Fig. 15 the minimum in x occurs at x = -0.166 mm: the minimum y, at -0.064 mm.[18]

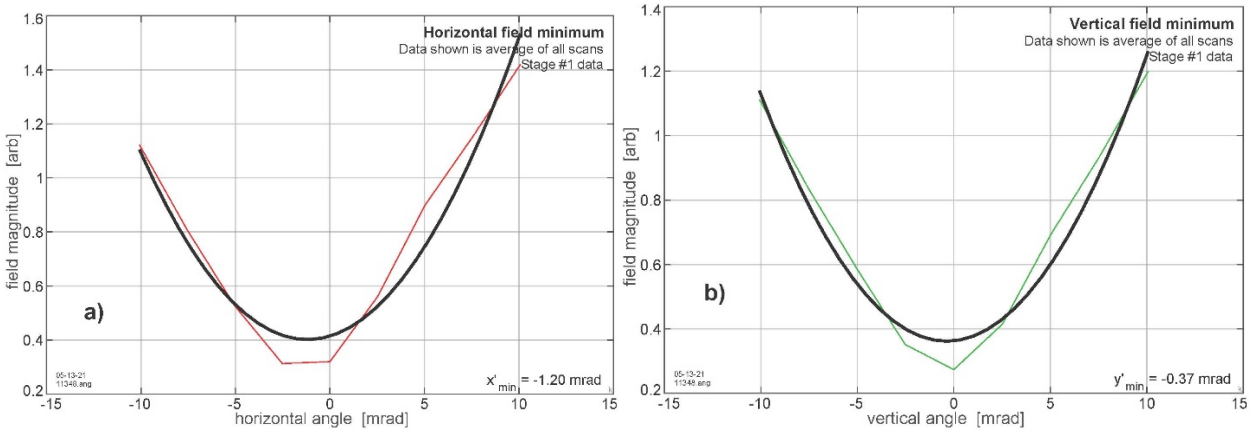

Figure 16. Measurement of a) the yaw (x') and b) the pitch (y') of the magnetic axis with respect to the solenoid mechanical axis.

A measurement of the yaw (x') and pitch (y') is shown in Figure 16. The vibrating wire was placed at x=0, y = 0 for these measurements. For the measurements shown in Fig. 16 the x' minimum occurs at about -1.20 mrad; the y' minimum, at about -0.37 mrad.[18] The SWAT results presented in Figs. 15 and 16 are for a right-handed coordinate system.

Diamagnetic Loop Calibration

In order to calibrate the two counter-wound diamagnetic loop we fabricated six ~46 cm long solenoids, two that are 1.59 cm diameter, one with 20 turns, the other with 40 turns; two that are 2.54 cm diameter, one with 20 turns, the other with 40 turns; and two that are 5.08 cm diameter, one with 20 turns, the other with 40 turns. See Table 5 for a list of approved drawings. The calibration coil wire diameter is 1.02 mm. A sketch of the 5.08 cm diameter, 20 turn calibration coil is shown in Fig. 17.

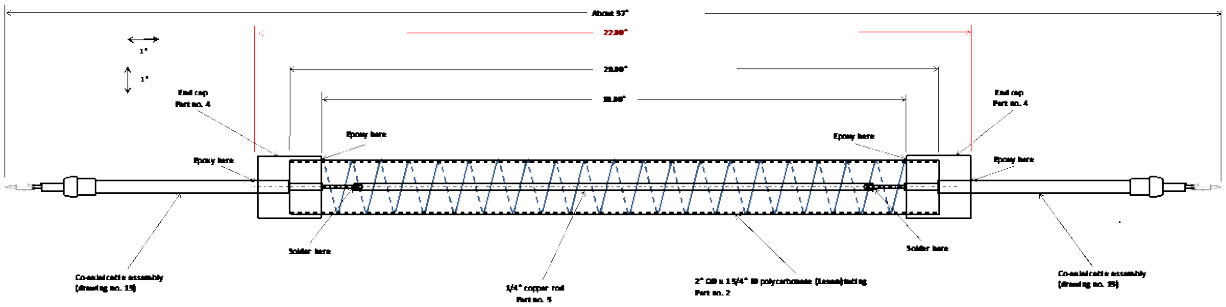

Figure 17. A sketch of the 5.08 cm diameter, 20 turn calibration coil.

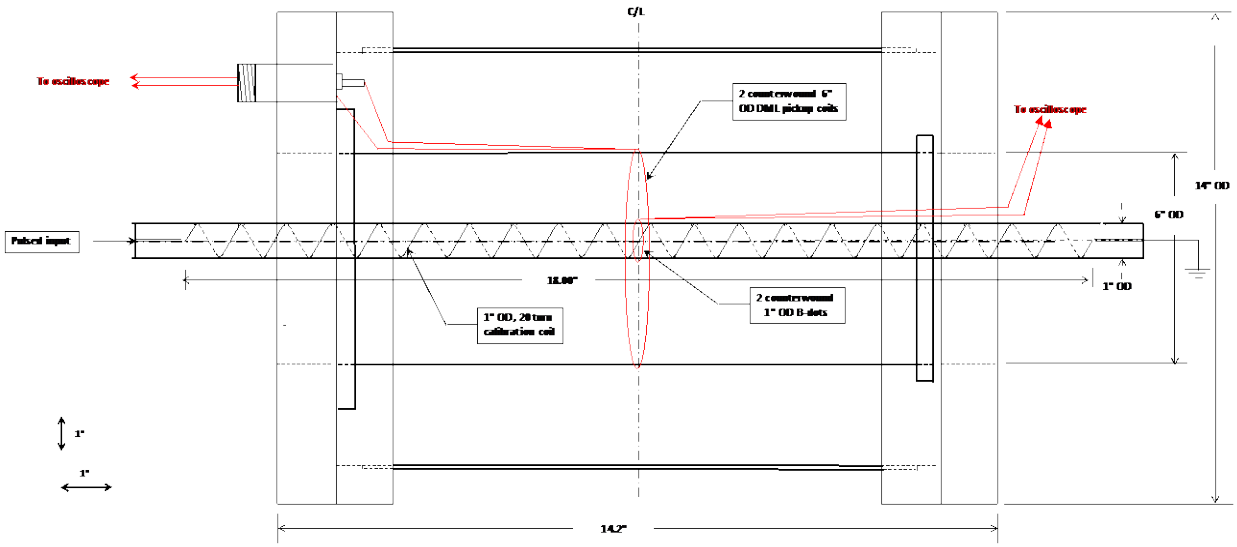

Figure 18. A sketch of the apparatus used to measure the calibration constant without the solenoid magnet is shown for the 2.54 cm diameter, 20 turn calibration coil. A 2-turn, counter-wound B-dot is used to measure the flux produced by that calibration coil.

Initially we attempted to calculate the inductance of the six calibration coils[19] so that we could calculate the B field, and thus the generated flux, but we gave up on that approach because of the large spacing between each turn of the solenoid. Instead we follow the approach in ref. 4 and place a 2-turn, counter-wound B-dot at the center of each of the six calibration coils. The B-dot wire diameter is 0.127 mm. A sketch of the experimental arrangement is shown in Fig. 18 for the 2.54 cm diameter, 20 turn calibration coil with a 2-turn, counter-wound B-dot used to measure the produced flux.

The measurements shown in Figs. 19-21 are without this assembly inserted into the solenoid magnet. For these measurements pulsed 1-5 V voltages are provided by an Agilent 33522A waveform generator and pulsed voltages of 7-700 V are provided by an AVTECH AVR-7B-B pulser. The pulse width is 400 ns. The DML signals are recorded with a LeCroy model HDO 8000A digital oscilloscope and post-processed using analysis software written in IDL.

The measured DML response for the 1.59 cm, 20 turn calibration coil when pulsed with a 100 V, 400 nsec wide pulse is shown in Fig. 19.

The integrated difference signals for the raw pulses displayed in Fig. 19 are shown in Fig. 20. The green curve is the integrated DML signal and the red curve is the integrated calibration coil signal. The calibration constant k is given by
k = $\int V_{DML} dt \,/\, \int V_{Loop} dt$, 0.661 for this measurement.

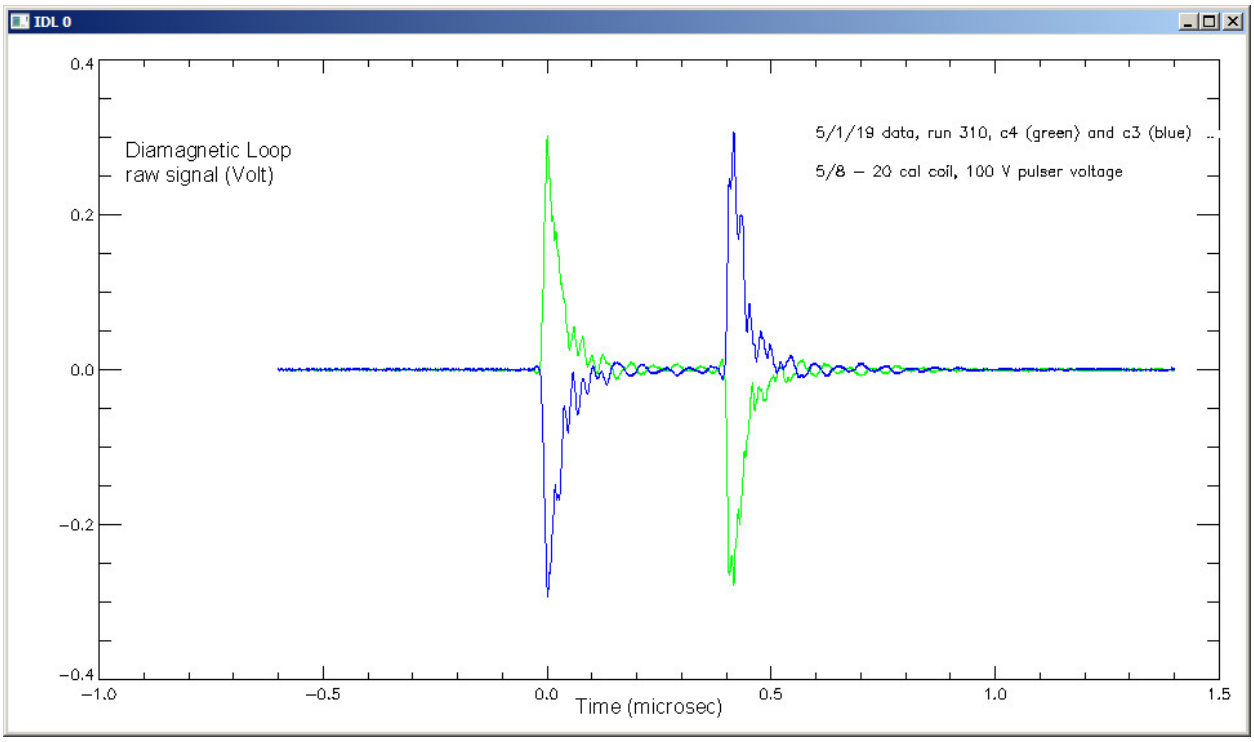

Figure 19. The measured DML response for the 1.59 cm, 20 turn calibration coil pulsed with a 100 V, 400-nsec-wide pulse. The green curve is for one of the diamagnetic loops and the blue curve is for the other (counter wound) diamagnetic loop.

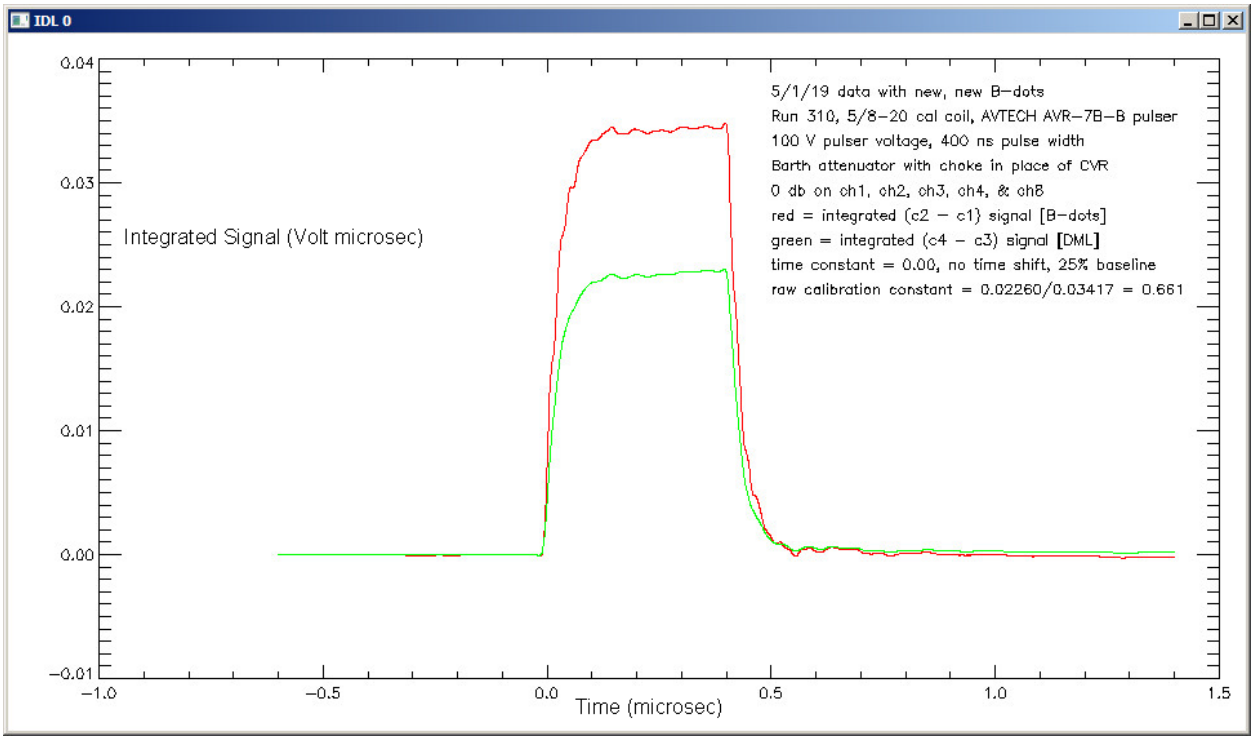

Figure 20. The integrated signals for the raw pulses displayed in Fig. 19 are shown in this figure (green curve). The calibration constant k = $\int V_{DML} dt \,/\, \int V_{Loop} dt$ = 0.661.

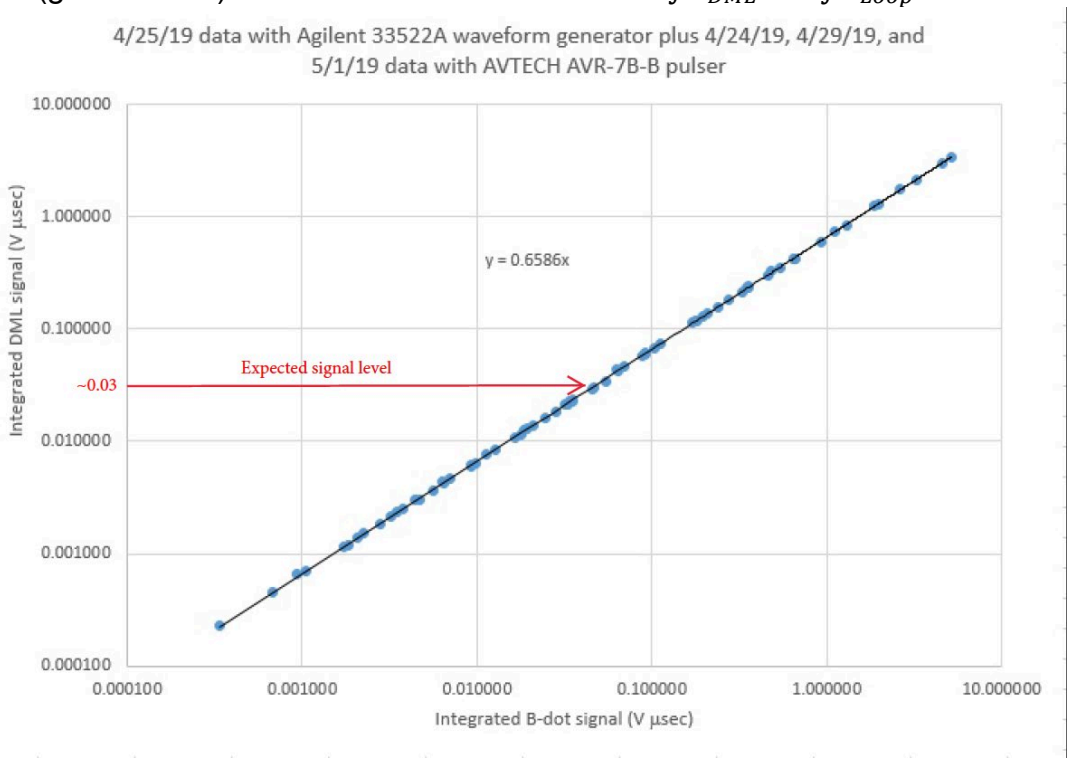

Figure 21. The calibration constant deduced from measurements of each of the six calibration coils, with pulser voltages ranging from 1 V to 700 V for the diamagnetic loop apparatus outside the solenoid magnet. The calibration constant k is the slope of the linear fit to the data, 0.659.

We measured the calibration constant for each of the six calibration coils, with pulser voltages ranging from 1 V to 700 V. The results of these measurements, 107 in all, are shown in Fig. 21.

A) 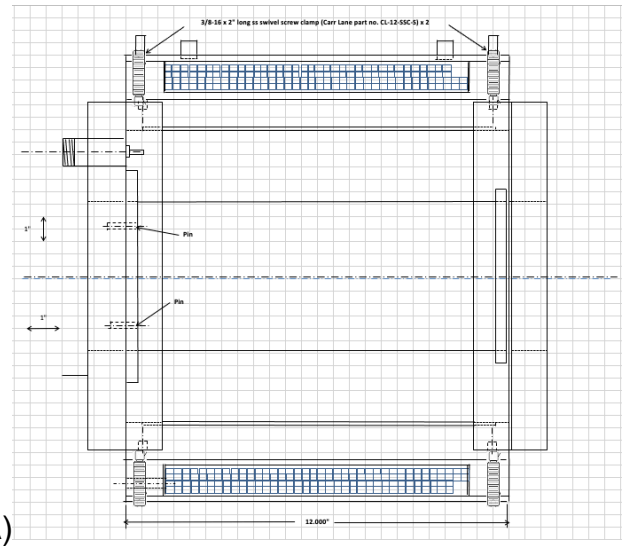

B) 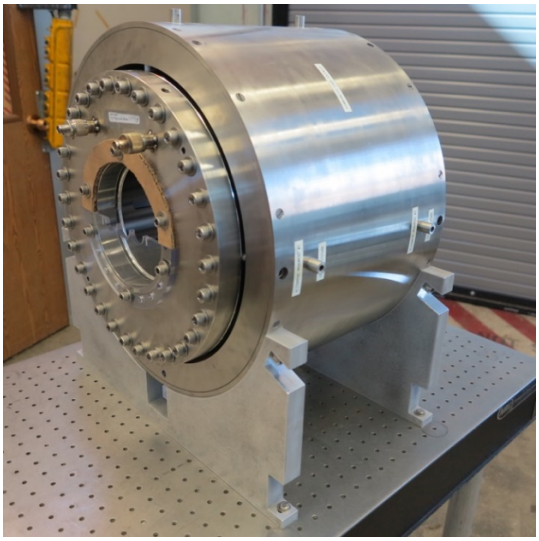

Figure 22. A) A sketch of the diamagnetic loop assembly inside the solenoid magnet. B) A photograph showing the diamagnetic loop assembly mounted inside the solenoid magnet.

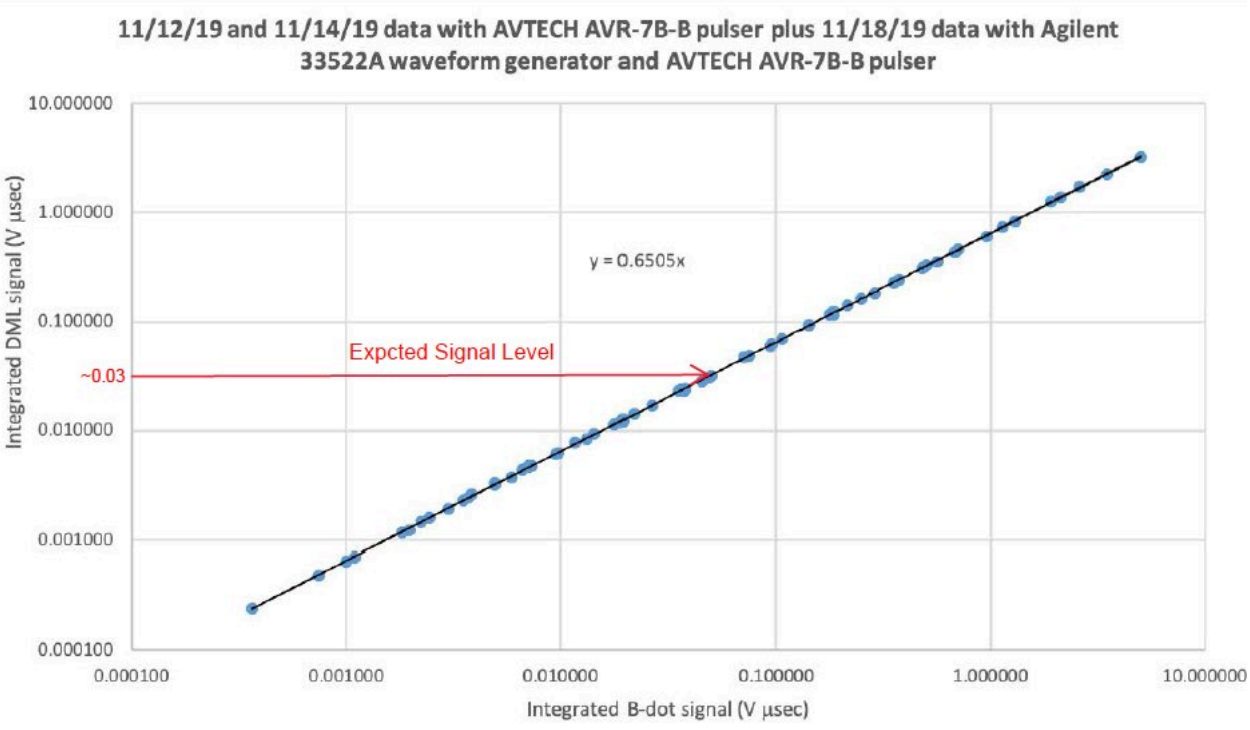

Figure 23. The calibration constant deduced from measurements of each of the six calibration coils, with pulsed voltages ranging from 1 V to 700 V for the diamagnetic loop apparatus inside the solenoid magnet with the magnet current = 70 A (B_z = 250 G). The calibration constant is the slope of the linear fit to the data, 0.651.

After the fabrication and mapping of the solenoid magnet were completed the diamagnetic loop apparatus was placed inside the solenoid magnet (Fig. 22).

The calibration measurements were repeated to ensure that the presence of a constant magnetic field does not change the calibration constant. For a solenoid magnet current of 70 A (B_z = 250 G) the results of the 68 measurements obtained using all 6 calibration coils are shown in Fig. 23. Pulser voltages ranged from 1 V to 700 V for these measurements which yielded a calibration constant k = 0.651. We use the average, k = 0.655, of the measured k without the solenoid, 0.659, and with the solenoid, 0.651, for the calibration constant of this device.

Potential Electron Beam Offset-Tilt Contribution to the Measured DML Signal

If there is only longitudinal (z direction) motion of the electron beam (no r or theta velocity component) there is no induced axial diamagnetic field and the signal from a diamagnetic loop apparatus is zero.[20] A tilt in r alone makes no contribution to the total flux through the loop, even if the beam is offset.

However, if the electron beam transits the DML off-axis and tilted it will produce a net B_z flux. If the probe has a pitch and/or yaw, and is off-center, then a DML signal proportional to xy' – x'y is generated.[3] Pure offset causes no error (X' = Y' =0, thus XY'-X'Y =0). Pure tilt of a beam centered on the loop causes no error (X = Y = 0, thus XY'-X'Y = 0).

We use the zero magnetic moment probe (Fig. 24) fabricated to measure the magnitude of the xy' – x'y signal. Six different semi-circular calibration probe holders were used to make the measurements shown in Fig. 24. Two had three 2.54-cm-diam. holes on the y = 0 centerline with x = -3.0 cm, 0 cm, and +3.0 cm; two had three 2.54-cm-diam. holes with y = +3.0 cm and x = -3.0 cm, 0 cm, and +3.0 cm; and two had three 2.54-cm-diam. holes with y = -3.0 cm and x = -3.0 cm, 0 cm, and +3.0 cm. The calibration probe holder with y = 0 cm is shown in the photograph in Fig. 6. Two of these calibration probe holders, separated by 36.17 cm, are used for these measurements. The maximum xy'-yx' available with this arrangement is 4,991 mm mrad. By using combinations of these 6 calibration probe holders a 9 x 9 array with 81 combinations can be mapped out, the majority of which are rotationally symmetric and thus duplicates.

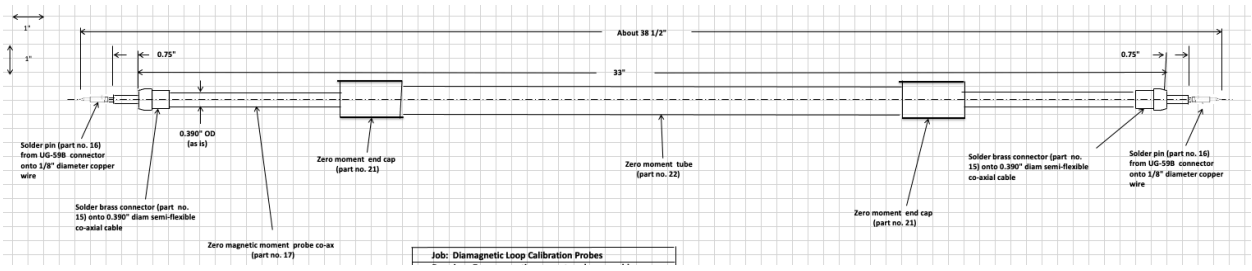

Figure 24. A sketch of the zero magnetic moment probe fabricated to measure the magnitude of the xy' – x'y signal.

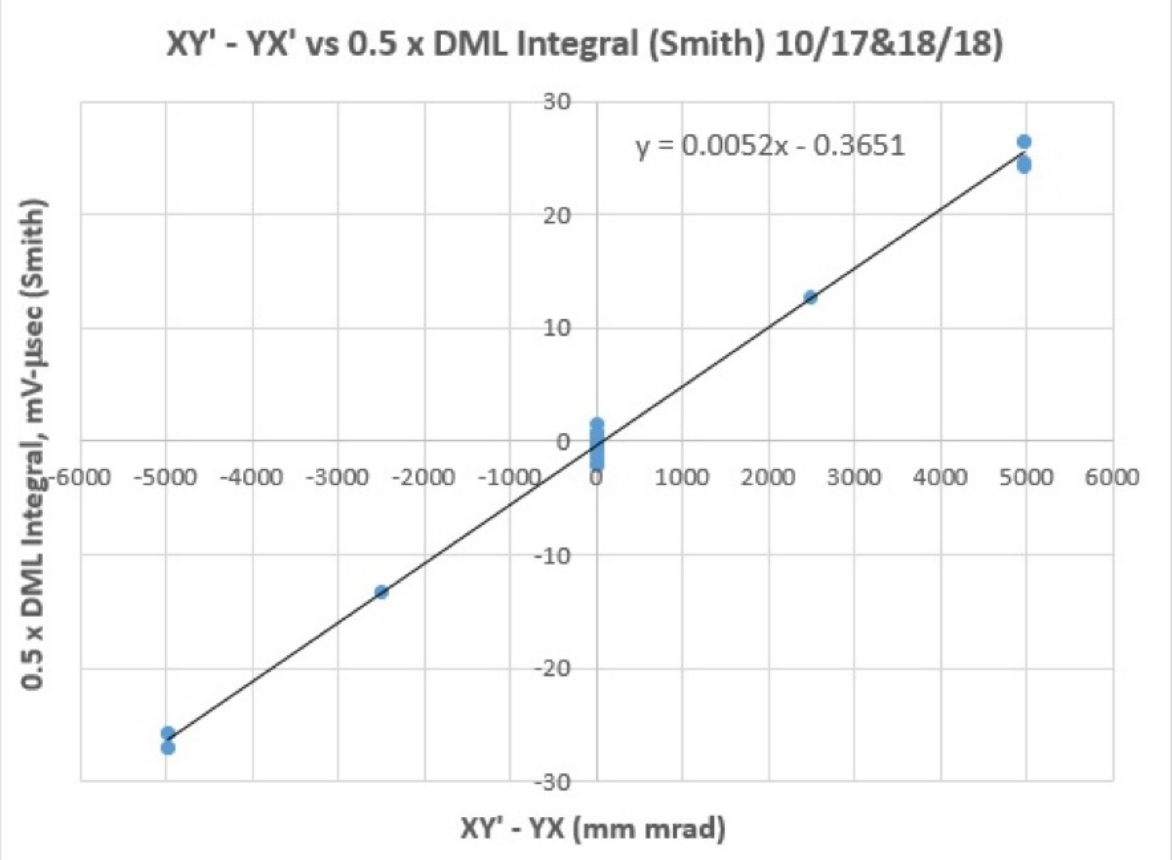

Figure 25. The measured response of the diamagnetic loop to the xy' – x'y tilt/offset of the zero magnetic moment probe.

As shown in Fig. 25 the present measurements confirm the predicted xy' – x'y dependence. 5,000 mm mrad produces 52 mV μsec for 14 A pulsed current. The error is 0.74 μV μsec per 1 mm mrad per 1 A compared to the expected value of 0.63 μV μsec per 1 mm mrad per 1 A (Appendix A). For a 1700 A DARHT-I e^- beam with 1 mm mrad "misalignment" the predicted addition to the DML signal is 1.3 mV μsec. This is ~4% of the expected 30 mV μsec diamagnetic loop signal.

DARHT-I Beam Size Measurement

The rms beam radius measured with a diamagnetic loop in an ideal geometry having no axial or azimuthal dependence, and with uniform field is[11]

$$R_{rms} = \sqrt{\frac{\mathrm{I_A}}{2\,\pi\,\mathrm{B}_z\,I_z\,\left[1-\frac{R_{loop}^2}{R_{wall}^2}\right]}\int V_{DML}(t)dt} \qquad (3)$$

In the derivation of eq. 3 the term $[1 - R_{loop}^2/R_{wall}^2]$ assumes a mandrel of infinite length and non-conducting material through which the time varying field penetrates

unimpeded. Since the conducting beam pipe (and mandrel) have a magnetic skin depth much shorter than its thickness at the frequencies of interest, only a fraction of the total field penetrates through the slots, reducing this factor by about 10%. Thus it is necessary to replace the factor $[1 - R_{loop}^2/R_{wall}^2]$ with the measured calibration factor k, 0.655, discussed above. It is satisfying that the value of k = 0.655 is close to the value of $[1 - R_{loop}^2/R_{wall}^2] = 0.72$, a 10% difference.

Replacing $[1 - R_{loop}^2/R_{wall}^2]$ with k results in eq. 4

$$R_{rms} = \sqrt{\frac{\mathrm{I_A}}{2\,\pi\,B_z\,I_z\,\mathrm{k}}\int V_{DML}(t)dt} \qquad (4)$$

For a hypothetical 20 MeV, 1.7 kA DARHT-I electron beam the rms beam size can be calculated using eq. 4 and the following parameters: I_A = 17.05 $\beta\,\gamma$ kA = 17.05 x 1 x 39.7 kA, $\int V_{DML}dt$ = 0.03 V μs, B_z = 0.01 T, I_z = 1.7 kA, and k=0.655. The rms beam size for this example is R_{rms} = 1.7 cm. The value used for $\int V_{DML}dt$, 0.03 V μs, is the expected integrated diamagnetic loop signal strength.

Corrections That Need to be Made

The calibration coils are not infinitely long, and the flux-conserving can is finite length. Moreover, there were no adjoining beam pipes attached during calibration. The finite length of the can is inherent to the measured calibration factor, but a correction is needed for the length of the coil and the beam pipes. These finite length corrections have been calculated with the PerMag magnetic field code.[21] The magnetic field produced by a current sheet solenoid with the dimensions of the 1-inch calibration coil for the calibration geometry (Fig. 26) and for the addition of the beam pipes (Fig. 27). For each of these, the calibration factor *k* was deduced from fluxes linking the DML and coil as calculated by PerMag. The ratio of the two gives the correction factor needed for adding the beam pipe. Furthermore, an additional simulation with the calibration coil four times as long was performed. Again, comparing calibration factors deduced from the simulated fluxes gives the total correction due to both adding beam pipe and increasing the coil length to better approximate the beam. Since adding beam pipe decreases *k*, and increasing coil length increases *k*, these corrections almost cancel; the net correction is that the *k* must be increased by 1.0%.

Since these simulations were azimuthally symmetric, they did not account for the slotted mandrel or leakage flux from the loosely wound calibration coil. The slotted mandrel effect is inherent in the measured calibration factor, but the leakage flux is not, and will be the subject of future 3D simulations.

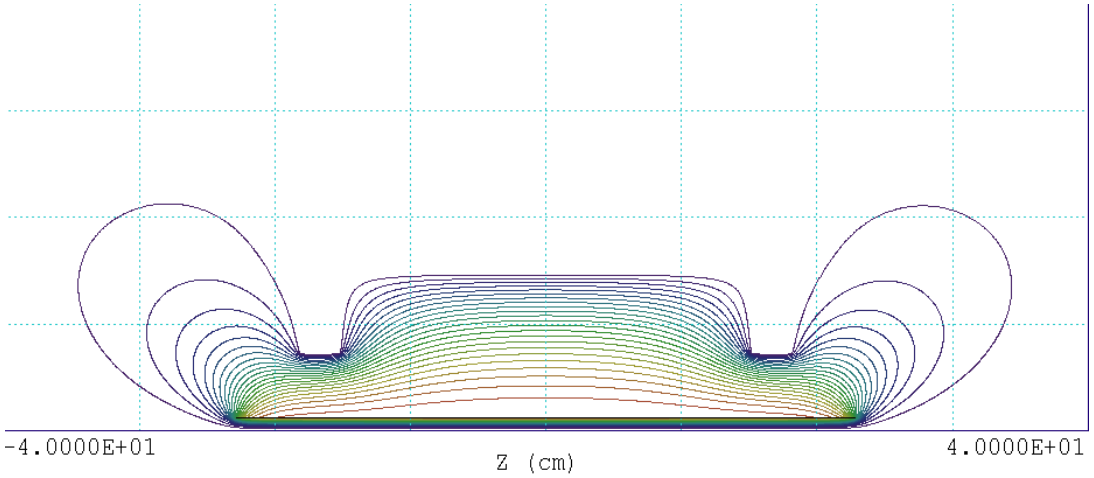

Figure 26. Magnetic flux calculated by PerMag for the 1-inch calibration coil in the DML can as configured for calibrations.

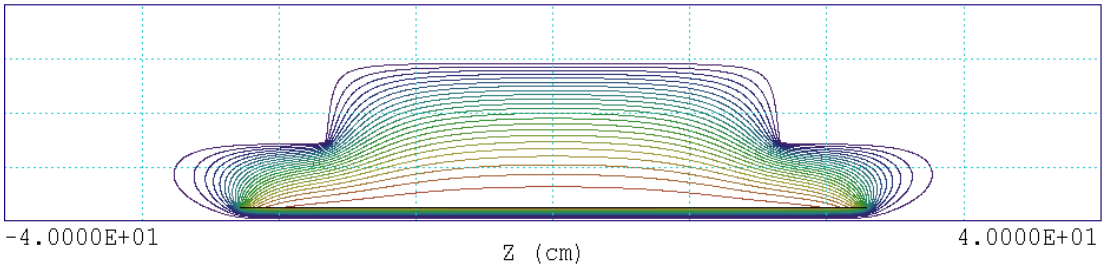

Figure 27. Magnetic flux calculated by PerMag for the 1-inch calibration coil in the DML can with beam pipe attached.

The xy' – x'y effect will add a spurious signal to the recorded $\int V_{DML}(t)dt$ signal. Once the DML is installed on a DARHT beamline we will need to measure the magnitude of this spurious signal and correct $\int V_{DML}(t)dt$ for it. The correction can be established from zero B-field measurements of beam-induced DML signal. Correction can be minimized by steering the beam to minimize the zero B-field measurements of the beam-induced DML signal.

The real limitations on the accuracy of this beam size diagnostic will come from the difficulties encountered in operating and recording the signals in a hostile pulsed-power environment: we won't be able to assess those limits until we install and test this device on one of the DARHT accelerators.

Discussion

Like all physical measurements, the DML beam-size result has errors, uncertainties, and corrections. Errors due to violation of experimental controls are expressed as errors in excluded flux. For example, error due to an un-centered beam. Uncertainty due to poor signal-to-noise is also expressed as uncertainty in excluded flux. Poor S/N was the nemesis of early DARHT-II loop measurements. The present DML apparatus

was specifically designed to improve the signal-to-noise. Theory linking excluded flux measurement to beam radius is subject to corrections due to violation of the assumptions. Corrections due to finite length of solenoid, flux conserving surface, and length of calibration coil can be calculated from magnetic field simulations – these calculations are in progress.

Conclusions

We have designed, built, and calibrated an electron beam radius monitor based on ref. 11. The calibration constant k is 0.655. This device is now ready to be installed on an electron induction LINAC and tested with a beam of known radius so that the accuracy of the beam radius measured using it can be assessed.

Acknowledgements

Many people helped to make this diamagnetic loop beam size diagnostic a real device – their contributions are listed in Table 1. We are especially indebted to Martin Schulze and Walter Tuzel for help with the solenoid magnet design, Sharon Dominguez for making the fabrication drawings, Rudy Valdez for leak checking this device, the AOT-MDE magnet fabrication team for mapping the solenoid magnet, and the AOT-AE/AOT-MDE teams for determining the magnetic axis of the solenoid magnet.

References

1) W. E. Nexsen, “Beam Brightness from Beam Diamagnetism,” Lawrence Livermore National Laboratory Research Memo No. 87-27, 1987 (unpublished).
2) W. E. Nexsen, “Status of Beam Diamagnetism Measurements,” Lawrence Livermore National Laboratory Research Memo No. 88-18, 1988 (unpublished).
3) W. E. Nexsen, “A Non-Interfering Beam Radius Diagnostic,” Lawrence Livermore National Laboratory Report UCRL-JC-108211, 1991 (unpublished).
4) W. E. Nexsen, “A Non-Interfering Beam Radius Diagnostic Suitable for Induction Linacs,” UCRL-TR-213331, 2005 (unpublished). http://oa.las.ac.cn/oainone/service/workdown/RO201907010014170LZ
5) W. E. Nexsen, et. al., “Reconstruction of FXR Beam Conditions,” Proceedings of the 2001 Particle Accelerator Conference, pp 2383-5. https://accelconf.web.cern.ch/p01/PAPERS/WPAH127.PDF
6) C.A. Ekdahl, et al., “Non-invasive measurements of intense relativistic electron beam size,” 42nd Annual Meeting of the APS Division of Plasma Physics, Quebec City, Canada, October 23-27, 2000. LA-UR-00-4982.
7) Fan Mu, “Study on the Diagnosis of the Radius of an Intense Pulsed Electron Beam by Use of a Diamagnetic Loop,” Master’s thesis, Chinese Academy of Engineering Physics, 2004 (in Chinese). Available from https://www.dissertationtopic.net/down/1280523
8) Fan Mu, et al., “Diamagnetic Loop Diagnoses the 2 MeV Injector Beam Radius,” Chinese Physics C, Volume 30, Supplement 1, 2006, pp. 87-89. http://cpc.ihep.ac.cn/article/id/cbc97713-fead-4519-b929-5d703857db8d#FullText_View
9) Fan Mu, et al., “Diamagnetic Loop Diagnoses Emittance of Intense Pulse Beam,” proceedings of the 17th International Conference on High Power Particle Beams (BEAMS 2008). https://ieeexplore.ieee.org/stamp/stamp.jsp?tp=&arnumber=6202895
10) G-J Yang, et al., “Beam Measurement of the Dragon-I Linear Induction Accelerator,” Chinese Physics C, Volume 30, Supplement 1, 2006, pp 105-7. http://cpc.ihep.ac.cn/article/id/5be40ae4-0006-4d93-b1a8-ee4a2b6ef329#FullText_View
11) C. Ekdahl, “Noninvasive measurement of electron-beam size with diamagnetic loops,” Rev. Sci. Instrum., Volume 72, Number 7, 2001, pp 2909-2914. https://aip.scitation.org/doi/pdf/10.1063/1.1379605
12) C.A. Ekdahl, “A Non-Invasive Beam Size Diagnostic for ARIA,” LANL report no. LA-UR-14-22420 (April 2014). https://permalink.lanl.gov/object/tr?what=info:lanl-repo/lareport/LA-UR-14-22420
13) R. Valdez, Los Alamos National Laboratory, private communication.
14) M. J. Burns et al., “Magnet Design for the DARHT Linear Induction Accelerators,” Proceedings of the 1991 Particle Accelerator Conference, pp 2110-2. https://accelconf.web.cern.ch/p91/PDF/PAC1991_2110.PDF
15) B. Feinberg et al., “A Method for Improving the Quality of the Magnetic Field in a Solenoid,” Nuclear Instruments and Methods in Physics Research, vol. 203 (1982) pp 81-85. https://reader.elsevier.com/reader/sd/pii/0167508782906123?token=1EAA3551B48

C9536F0E6BAADBA9A91517ADE3AF5B2BC1DE23AC4376433599C066E042CEA3BA95218718A8DF0790B7BC5
16) Henry Gaus III, AOT-RFE Tech Note 19-004, September 10, 2019.
17) M. E. Schulze, Los Alamos National Laboratory, private communication.
18) Kip Bishofberger, Los Alamos National Laboratory, private communication.
19) Frederick W. Grover, Inductance Calculations: Working Formulas and Tables, Dover Publications, Inc., New York, 1946.
20) B. E. Carlsten, "Using the Induced Axial Magnetic Field to Measure the Root Mean Square Beam Size and Beam Density Uniformity of an Electron Beam in an Induction LINAC," Rev. Sci. Instrum., Volume 70, Number 8, 1999, pp 3308-3313. https://aip.scitation.org/doi/pdf/10.1063/1.1149909
21) C, A. Ekdahl et al., "2D simulations of Diamagnetic Loop Calculations," LA-UR-21-21481 (2021). https://permalink.lanl.gov/object/tr?what=info:lanl-repo/lareport/LA-UR-21-21481

Tables

David J. Ballard	AOT-MDE	Laser tracker measurements for SWAT
Juan Barraza	ASD-TECH	Mechanical design
Kip A. Bishofberger	AOT-AE	SWAT
Nathaniel G. Bratt	PF-MFG	Mechanical fabrication
M. Anthony Chavez	ASD-TECH	Mechanical design
Joshua E. Coleman	J-6	Technical guidance and support
Sharon A. Dominguez	J-6	Mechanical design and CAD drafting
Ryan L. Fleming	AOT-AE	SWAT
Henry Gaus III	AOT-RFE	Solenoid mapping
Jeffrey B. Johnson	J-6	Technical guidance
Nathan Kollarik	AOT-MDE	Laser tracker measurements for SWAT
Rodney C. McCrady,	AOT-AE	Technical guidance
Aaron McEvoy	NSTEC	Experimental measurements
Jacob L. Medina	AOT-MDE	Solenoid fabrication and documentation
Jeffrey M. Montgomery	NSTEC	Experimental measurements
P. Daniel Olivas	J-6	Mechanical assembly, electrical support
Mario A. Pacheco	AOT-MDE	Solenoid fabrication and assembly
Austin R. Patten	J-6	Solenoid mapping
Donald G. Roeder	PF-MFG	Mechanical fabrication
Brandon J. Roller	AOT-MDE	Solenoid design, fabrication, and assembly
Gary P. Salazar	J-4	Mechanical design for laser tracker alignment
Manolito Sanchez	J-6	Mechanical assembly, documentation
Jacob B. Sandoval	AOT-RFE	Solenoid Mapping
Martin E. Schulze	J-6	Solenoid design
Rudolph J. Valdez,	J-6	Vacuum support, leak detection
Alexander J. Wass,	AOT-MDE	SWAT
Walter M. Tuzel	J-6	Diamagnetic loop and solenoid design

Table 1. People who made significant contributions to this work and their contribution.

Parameter	Symbol	Units	Value
DML mandrel			
Inner radius[a]		cm	7.30
Outer radius[b]		cm	7.94
DML mandrel slots	N_s		8
Slot length[c]	L_s	cm	25.40
Slot width[d]	w_s	cm	1.27
DML vacuum housing			
Inner radius[e]	R_{wall}	cm	14.92
Inner length[f]	L_{wall}	cm	30.48
Flux Loop			
Radius[g]	R_{loop}	cm	7.916
Cu wire diameter[h]		cm	0.1024
Solenoid magnet			
Inner radius[i]		cm	19.08
Outer radius[j]		cm	21.73
Length[k,m]	L	cm	24.02
Number of turns/cm	n	turns/cm	5.50
Number of turns[m]		turns	132

[a] The beam pipe inner diameter is 5.750” so the inner radius is 7.303 cm

[b] The beam pipe outer diameter is 6.250” so the outer radius is 7.938 cm

[c] The slot length is 10.000” (25.40 cm) with the middle 9.500” having parallel sides and the two 0.250” radius ends accounting for the remaining 0.500”

[d] The slot width is 0.500” = 1.27 cm

[e] The inner diameter is 11.75” so the inner radius is 14.923 cm

[f] The sensing can is 12.00” long = 30.48 cm

[g] The outer radius of the copper wire loop (accounting for the insulation thickness)

[h] The thickness of the copper wire (excluding the insulation thickness)

[i] The inner radius of the windings is 7.50” = 19.05 cm: adding 0.0127 cm sheet insulation and 0.0165 cm wire insulation gives 19.08 mm for the inner radius

[j] The radius of the 4 windings of 0.668 cm thick square magnet wire less the thickness of the outer insulation layer (0.0165 cm) added to the 19.08 cm inner radius gives 21.73 cm

[k] Takes into account one 0.005” spacer on each end of the magnet windings, 0.010“ total

[m] There are 34 turns on each of the two inner windings and 32 turns on each of the two outer windings. Note that the outer windings are off-center of the magnet.

Table 2. Dimensions for the diamagnetic loop apparatus and for the solenoid magnet.

Drawing Number	Drawing Title	Description
47Y1773267_1B	Diamagnetic Loop Assembly	Assembly sheet 1
47Y1773267_2B	Diamagnetic Loop Assembly	Assembly sheet 2
47Y1773268_1A	Diamagnetic Loop Outer Tube Weldment	Outer housing sheet 1
47Y1773268_2A	Diamagnetic Loop Outer Tube Weldment	Outer housing sheet 2
47Y1773269_1B	Diamagnetic Loop Current Return Weldment	DML mandrel
47Y1773269_2B	Diamagnetic Loop Current Return	DML mandrel
47Y1773270_1A	Diamagnetic Loop 14” Flange	Flange w/ type N connectors, sheet 1
47Y1773270_2A	Diamagnetic Loop 14” Flange	Flange w/ type N connectors, sheet 2
47Y1773295_1A	Diamagnetic Loop 14” Flange	Other flange sheet 1
47Y1773295_2A	Diamagnetic Loop 14” Flange	Other flange sheet 2
47Y1773551_1A	Diamagnetic Loop Plate	Calibration plate
47Y1773552_1A	Diamagnetic Loop Cradle	Assembly support
47Y1773553_1A	Diamagnetic Loop Plate	Calibration plate clamp
47Y1773589_1A	Diamagnetic Loop Weldment Assembly	Type N connector welds
47Y1773657_1A	Diamagnetic Loop Vented Dowel Pin	Pins for vacuum use
47Y1925042_1A	Diamagnetic Loop Clamp 1	Clamp for transport
47Y1925118_1A	Diamagnetic Loop Clamp 2	Clamp for transport

Table 3. Diamagnetic loop vacuum assembly approved drawings.

Drawing Number	Drawing Title	Description
47Y1773374_1B	Diamagnetic Loop Solenoid Magnet Assembly	Assembly drawing
47Y1773375_1A	Diamagnetic Loop Solenoid Magnet Spool	Sheet 1
47Y1773375_2A	Diamagnetic Loop Solenoid Magnet Spool	Sheet 2
47Y1773554_1A	Solenoid Magnet Fiducial Rod	Holder for SMR target
47Y1773555_1A	Solenoid Magnet Housing	Sheet 1
47Y1773555_2A	Solenoid Magnet Housing	Sheet 2
47Y1773556_1B	Solenoid Magnet Cradle	Assembly support
47Y1922486_1A	Diamagnetic Loop Solenoid Magnet Ring	Insulator for windings
47Y1922525_1A	Solenoid Magnet Housing Weldment	Fiducial holder welded to housing
47Y1922526_1A	Diamagnetic Loop Solenoid Magnet Inner Loop Clamp	Clamp for holding inner windings
47Y1922527_1A	Diamagnetic Loop Solenoid Magnet Outer Loop Clamp	Clamp for holding outer windings
47Y1925045_1A	DML Solenoid Magnet SWAT Alignment Tool	Magnet SWAT alignment tool
47Y1925046_1A	Solenoid Current Lead Mounting Plate 1	Connector for magnet power supply
47Y1925047_1A	Solenoid Current Lead Mounting Plate 2	Connector for 2 solenoid loops
47Y1924679_1A	DML Solenoid Assembly with Cradle	Assembly drawing with cradle

Table 4. Diamagnetic loop solenoid magnet approved drawings.

Drawing Number	Drawing Title	Description
47y1922723_1A	Diamagnetic Loop Calibration Probe 2” OD Tube 20 turns	2-20 cal probe tube
47y1922724_1A	Diamagnetic Loop Calibration Probe 2” OD Tube 40 turns	2-40 cal probe tube
47y1922725_1A	Diamagnetic Loop Calibration Probe 2” Diameter Cap	2” cal probe end cap
47y1922732_1A	Diamagnetic Loop Calibration Probe 1” OD Tube 20 turns	1-20 cal probe tube
47y1922733_1A	Diamagnetic Loop Calibration Probe 1” OD Tube 40 turns	1-40 cal probe tube
47y1922734_1A	Diamagnetic Loop Calibration Probe 1.25” Diameter Cap	1” cal probe end cap
47y1923044_1A	Diamagnetic Loop 1” Calibration Probe Holder	1” hole on center
47y1923045_1A	Diamagnetic Loop 2” Calibration Probe Holder	2” hole on center
47y1923046_1A	Diamagnetic Loop Calibration Probe Clamp	Cal probe clamp
47y1923047_1A	Diamagnetic Loop Calibration Probe Brass Connector	Fitting for cal probe connector assmbly
47y1923048_1A	Diamagnetic Loop Calibration Probe Semi-Flex Co-Axial Cable	Cable for cal probe connector assmbly
47y1923053_1A	Diamagnetic Loop Calibration Probe Copper Rod	Rod connector
47y1923054_1A	Diamagnetic Loop Calibration Probe Co-Axial Cable	Connector assmbly
47y1923056_1A	Diamagnetic Loop Calibration Probe 2” Dia 40 Turns Assembly	2-40 cal probe assembly
47y1923058_1B	Diamagnetic Loop Calibration Probe 2” Dia 40 Turns	2-40 cal probe assy
47y1923083_1A	Diamagnetic Loop Calibration Probe 2” Dia 20 Turns Assembly	2-20 cal probe assembly
47y1923085_1A	Diamagnetic Loop Calibration Probe 1” Dia 40 Turns	1-40 cal probe assy
47y1923086_1A	Diamagnetic Loop Calibration Probe 1” Dia 20 Turns Assembly	1-20 cal probe assembly
47y1923087_1B	Diamagnetic Loop Calibration Probe 2” Dia 20 Turns	2-20 cal probe assy
47y1923088_1B	Diamagnetic Loop Calibration Probe 1” Dia 40 Turns	1-40 cal probe assy
47y1923089_1B	Diamagnetic Loop Calibration Probe 1” Dia 20 Turns	1-20 cal probe assy
47y1923404_1A	Diamagnetic Loop 0 Moment Cal Probe End Cap	0 moment end cap
47y1923405_1A	Diamagnetic Loop Cal 1” Cal Probe Holder 0 Offset, 3 Holes	3 1” holes, no offset
47y1923406_1A	Diamagnetic Loop Cal 1” Cal Probe Holder, + Offset, 3 Holes	3 1” holes, + offset
47y1923407_1A	Diamagnetic Loop Cal 1” Cal Probe Holder, - Offset, 3 Holes	3 1” holes, - offset
47y1923408_1A	Diamagnetic Loop 0 Moment Cal Probe Tube	Tube for assembly
47y1923409_1A	Diamagnetic Loop Zero Moment Cal Probe Assembly	0 moment probe assy w/ connectors
47y1923516_1A	Diamagnetic Loop Zero Moment Cal Probe Assembly	0 moment probe assy cross section
47Y1924891_1A	Diamagnetic Loop 5/8” Cal Probe B-Dot Manifold Part 30	Upper 5/8” B-Dot manifold
47Y1924892_1A	Diamagnetic Loop 5/8” Cal Probe B-Dot Manifold Part 31	Lower 5/8” B-Dot manifold

47Y1924993_1A	Diamagnetic Loop Calibration Probe .625” Dia. 40 Turns	5/8-40 cal probe tube
47Y1924994_1A	Diamagnetic Loop Calibration Probe .625” Dia. 20 Turns	5/8-20 cal probe tube
47Y1924995_1A	Diamagnetic Loop 5/8” Diameter Cal Probe End Cap	5/8-20 cal probe end cap
47Y1924996_1A	Diamagnetic Loop 5/8” Cal Probe Holder 0 Offset, 3 Holes	5/8” hole on center
47Y1925002_1A	Diamagnetic Loop 1” Cal Probe B-Dot Manifold Part 28	Upper 1” B-Dot manifold
47Y1925003_1A	Diamagnetic Loop 1” Cal Probe B-Dot Manifold Part 29	Lower 1” B-Dot manifold
47Y1925043_1A	Diamagnetic Loop 2” Cal Probe B-Dot Manifold Part 32	Upper 2” B-Dot manifold
47Y1925044_1A	Diamagnetic Loop 2” Cal Probe B-Dot Manifold Part 33	Lower 2” B-Dot manifold
47y1925260_1A	Diamagnetic Loop Calibration Probe 0.625” Dia 20 turns	5/8-20 cal probe assembly
47y1925261_1A	Diamagnetic Loop Calibration Probe 0.625” Dia 40 turns	5/8-40 cal probe assembly

Table 5. Calibration coil approved drawings.

Appendix A

DML Signal Due to a Helical Beam Trajectory

An electron beam entering the field of a solenoid either at an angle or radially offset from the axis will execute a helical trajectory in the magnetic field. The axial field produced by this helical motion will produce a signal on the diamagnetic loop, so care must be taken to ensure that the beam is steered to be straight down the axis when entering the DML field to avoid this complication. This has been called the “offset-tilt” contribution to the DML signal. It can easily be understood from first principles, which compare favorably with measurements made on our apparatus.

The axial field produced by a beam with a helical trajectory can be approximated by the field of a long solenoid, $B_z = \mu_o n I$, where I is the current, n is the number of turns per unit length, and $\mu_o = 4\pi \times 10^{-7}$ H/m is the permeability of free space. The flux in this helix is $\Phi_h = B_z A_h = \mu_o n I \pi R^2$, where R is the helical radius. The pitch angle is found by considering that a single turn around the circumference ($2\pi R$) takes a length equal to 1/n, and therefore the pitch angle is given by $\tan\theta = 2\pi R n$. For small pitch angles, $\tan\theta \approx \theta \approx 2\pi R n$. Substituting into our formula for the flux gives $\Phi_h \approx \mu_o I R \theta / 2$.

In order to compare with measurements made during calibration of our DML one notes that the measured flux divided by the current, offset and tilt should give one half the permeability. From the measurements quoted one has 52nV-s /5m-mrad/14A = 7.43×10^{-7} H/m,[a] which is reasonably close to the expected value of 6.28×10^{-7} H/m, and well within the bounds of the approximations and experimental error. It should be noted that a more exact theoretical analysis of this effect was done by Richard Bartsch, with much the same result.

[a] 1 H/m = 1 Vs/Am